SLIDING MODE BASED FUZZY CONTROL FOR POSITIONING OF OPTICAL PICKUP HEAD

M. Y. Tsai and T. S. Liu

Department of Mechanical Engineering, National Chiao Tung University,

1001 Ta-Hsueh Rd., Hsinchu 30010, Taiwan, R.O.C.

E-mails: tsliu@mail.nctu.edu.tw

Abstract- A laser diode package is mounted on an optical pickup head actuator. The laser diode package is used to sense the displacement of a moving target by self-mixing interference signals. A sliding mode based fuzzy control method is developed to achieve fast response of the optical pickup head actuator, which is driven in a focusing direction. Simulation results show the proposed method performs better than sliding-mode control. Experimental results further show that the proposed control method outperforms sliding-mode control.

Index term*:* Sliding-mode control; fuzzy control; optical storage device; feedback lasers; photodiodes.

1. INTRODUCTION

In optical data storage, to read and write data, a pickup head actuator undergoes focusing, track-seeking, and track-following. Lee et al. [1] compared optical pickup head actuators using four-wire springs and two-wire springs. Furthermore, a two-wire suspension actuator is designed and analyzed for focusing motion.

Positioning control of an optical pickup head demands fast and accurate motion. Sliding-mode control (SMC) is popular with its robust and insensitive properties to matched disturbance and model uncertainty [2, 3]. Fuzzy control is a direct method for controlling a system without the need of a mathematical model, in contrast to the classical control which is an indirect method with a mathematical model [4, 5, 6]. In recent years, several studies have been done in order to combine the advantages of sliding-mode control and fuzzy logic. Hong et al. [7] developed a vehicle stability control system where the stabilizing yaw moment calculated using the SMC and the target slip determination method for generating the yaw moment constructed using the fuzzy logic. Yagiz et al. [8] improved ride comfort of passenger cars using active suspensions, and presented a new fuzzy logic sliding-mode control scheme where the slope constant in the robust nonchattering sliding-mode controller is tuned according to system states.

This study first introduces the system configuration of a laser diode (LD) package on an optical pickup head and describes how the LD package operates. Second, a sliding mode based fuzzy control is proposed to improve system performance. Sliding modes are used to determine parameters in fuzzy control rules, since robustness is inherent in a variable structure system with sliding modes. Compared with SMC, the proposed method results in smaller control effort and faster response in simulation results. Experimental results further show that shorter settling time and smaller displacement error are achieved.

2. SYSTEM CONFIGURATION

Fig. 1(a) shows a photo of a LD package inside an optical pickup head actuator with a focusing coil, a tracking coil, and a tilting coil [9]. A focusing coil with current generates Lorentz force and hence motion shown as dashed arrow in Fig. 1(a). The pickup head actuator moves with the LD package along the focusing direction. Hence, the LD package is positioned by tuning the focusing coil in the modified pickup head actuator.

Tracking coil connections are rewired to power the LD and provide electric connections to a photodiode (PD) sensor shown in Fig. 1(b). A reflector depicted in Fig. 1(a) is used to reflect laser beams. By using a laser Doppler vibrometer (LDV) in system identification, a transfer function from focusing coil voltage u to the vertical displacement y on the LD is identified as $Y(s)/U(s) = K\omega_n^2/(s^2 + 2\zeta\omega_n s + \omega_n^2)$, where gain $K = 2.64\times10^6$, damping ratio $\zeta = 0.28$, and resonant frequency $\omega_n = 48$ Hz. Fig. 2 depicts the corresponding Bode plot.

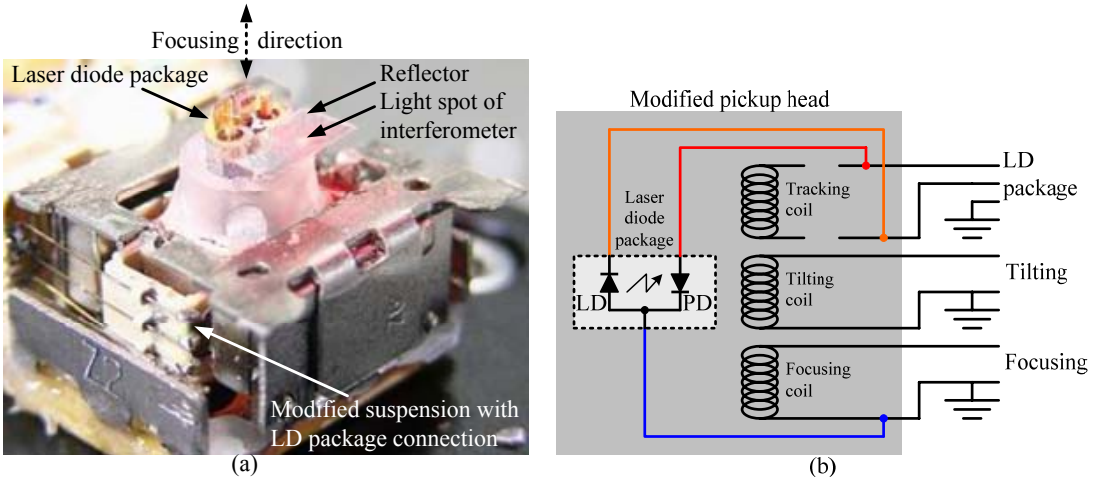

Fig. 1. (a) Photo of LD package inside optical pickup head actuator, (b) modified circuit for connection with LD package while disconnection of tracking coil.

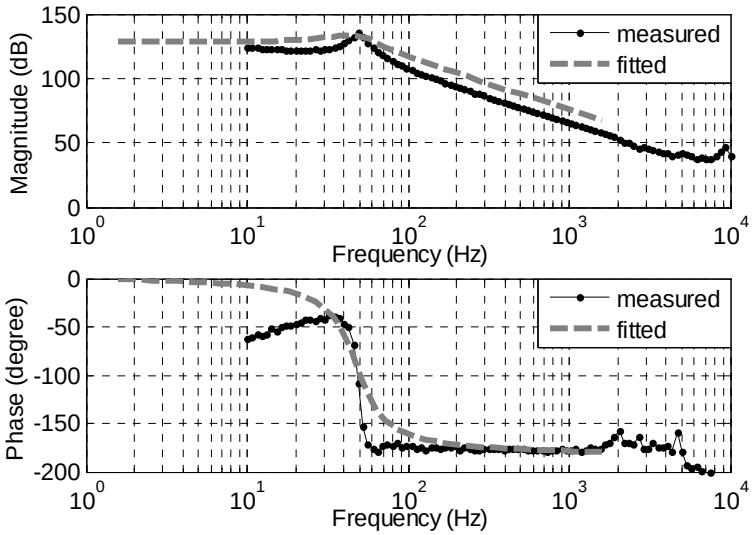

Fig. 2. Bode plot of focusing direction system.

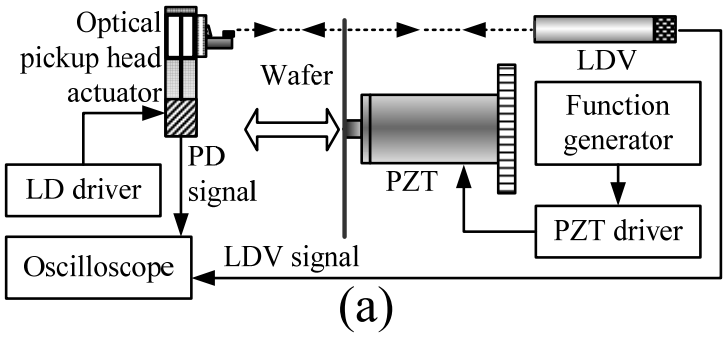

(a)

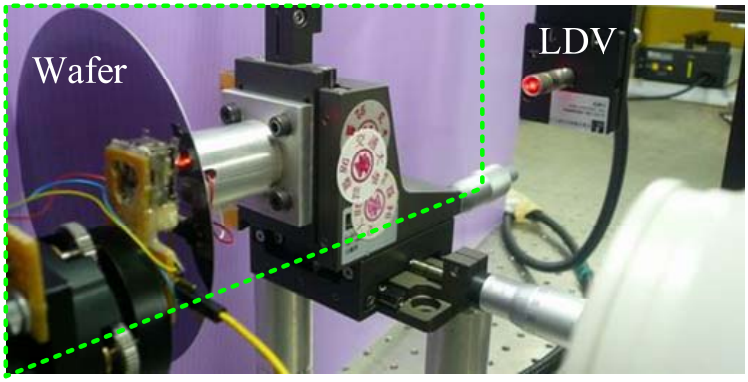

(b)

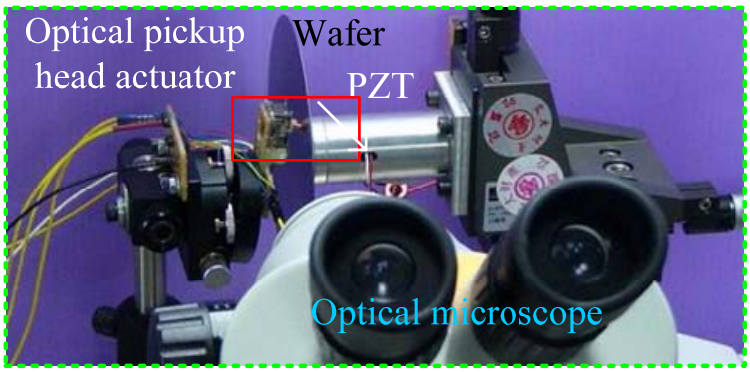

(c)

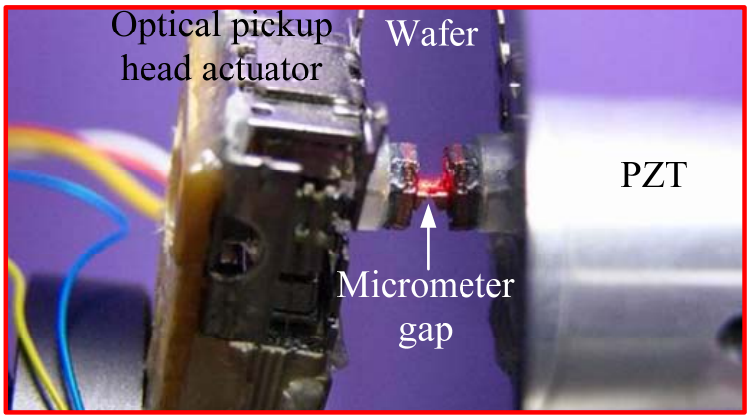

(d)

Fig. 3. (a) Experimental setup, (b) photo of a part in Fig. 3(a), (c) another photo for green dotted trapezoid in Fig. 3(b), and (d) enlargement from red block in Fig. 3(c).

For displacement sensing, self-mixing interference (SMI) systems constitute an alternative to conventional interferometers, since optical elements such as beam splitter, reference mirror, and photo detector are not required in SMI [10]. With both LD and PD, an actuated surface wafer is measured in the present system, as depicted in Fig. 3(a). The system consists of a modified pickup head actuator, a target wafer attached to a piezoelectric (PZT) actuator [11], and an LDV shown in Fig. 3(b). An optical microscope is utilized to observe the gap between the LD and the wafer shown in Figs. 3(c) and 3(d). The LD current is prescribed as 40 mA. Voltage amplitudes in the function generator are 2.54, 1.27, 0.635, 0.3175, and 0.15875 V with triangular waveform and 2 Hz frequency to enter the PZT driver for moving the PZT actuator. Oscilloscope channels one and two represent the SMI signal from PD port and the

LDV signal, respectively. Both sensors are used to measure displacement of a silicon wafer attached to the PZT actuator. Figs. 4(a), 4(b) 4(c), 4(d), and 4(e) show measured displacement of the silicon wafer where LDV signal in channel two is 2 μm per volt, and the SMI signal in channel one is $\lambda/2$ per complete interference fringe for a $\lambda = 635$ nm laser.

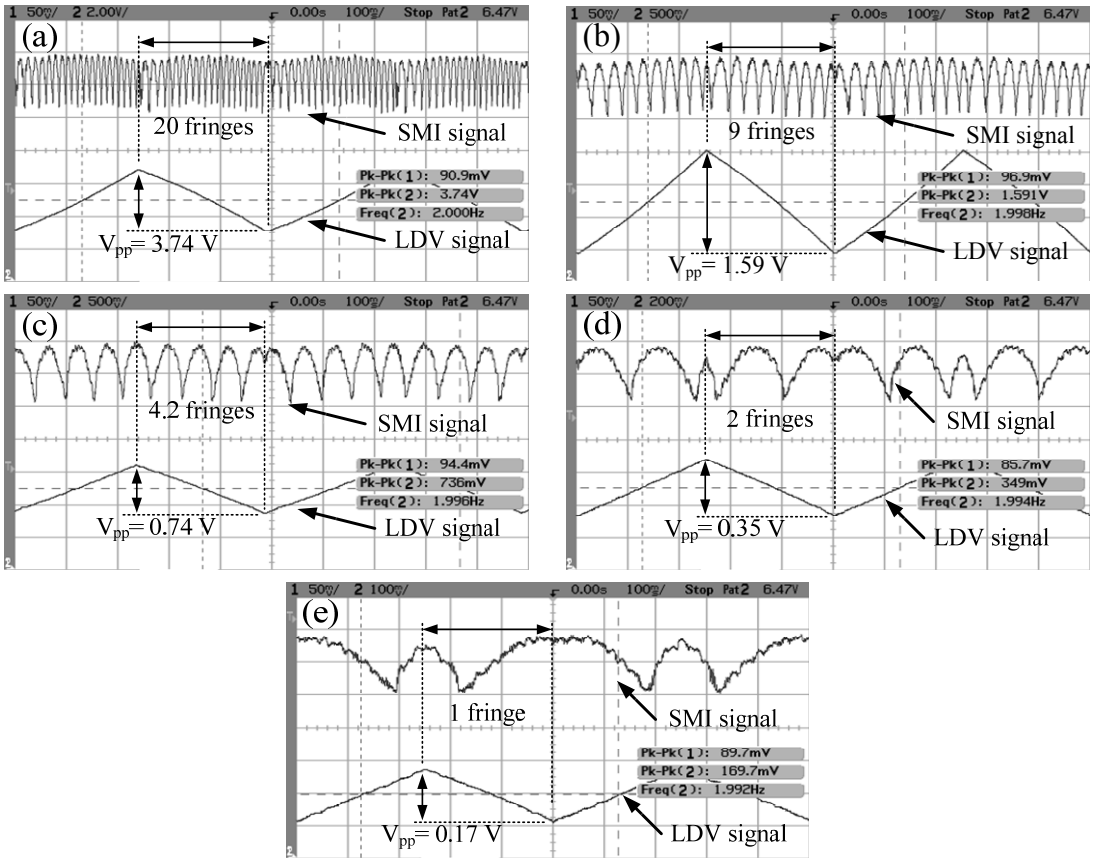

Fig. 4. Voltage signals of PZT displacement measured by PD and LDV, where input voltage amplitudes of PZT are 2.54 V in (a), 1.27 V in (b), 0.635 V in (c), 0.3175 V in (d), and 0.15875 V in (e).

Experimental results in Figs. 4(a), 4(b) 4(c), 4(d), and 4(e) are listed in Table 1. Concerning LDV and SMI signals, the larger amplitude in the LDV signal and the more fringes in the SMI signal there are, the larger displacement the silicon wafer attached to the PZT actuator undergoes. Moreover, Fig. 5 depicts that the shorter the PZT actuator displacement is, the less difference there is between LDV and SMI signals. Therefore, the LD package as a

displacement sensor on an optical pickup head actuator has the capability of displacement sensing demonstrated by LDV. In Section 3, the sliding mode based fuzzy control method will be proposed to control the position of the LD package on an optical pickup head actuator.

Table 1: Measured data obtained from Figs. 4(a), 4(b), 4(c), 4(d), and 4(e).

	SMI signal (fringe number)	0.3175 μm/fringe	LDV signal (V)	2 μm/V
Fig. 4(a)	20 fringes	6.35 μm	3.74 V	7.48 μm
Fig. 4(b)	9 fringes	2.857 μm	1.59 V	3.18 μm
Fig. 4(c)	4.2 fringes	1.334 μm	0.74 V	1.48 μm
Fig. 4(d)	2 fringes	0.65 μm	0.35 V	0.7 μm
Fig. 4(e)	1 fringe	0.318 μm	0.17 V	0.34 μm

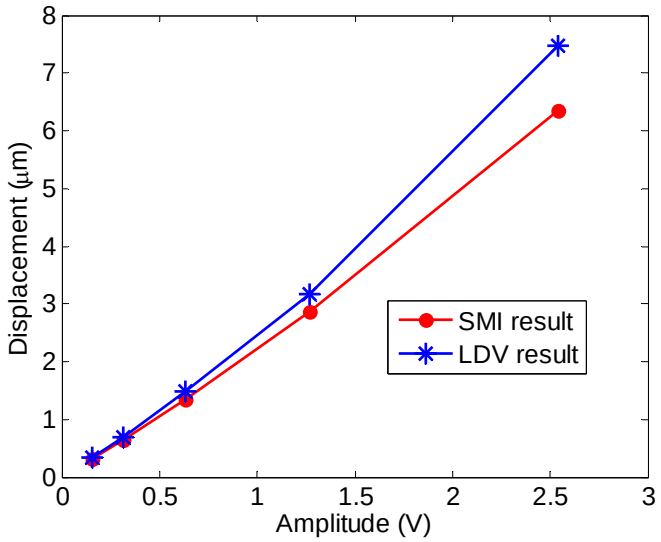

Fig. 5. Comparison between SMI and LDV results of PZT displacement.

3. SLIDING MODE BASED FUZZY CONTROL

3.1 Sliding-Mode Control

A variable structure system [12] can be described by $\dot{\boldsymbol{x}} = \boldsymbol{f}\left(\boldsymbol{x}, u(\boldsymbol{x})\right)$, where $\boldsymbol{x} \in \Re^n$ is state variables of the system and $u(\boldsymbol{x})$ denotes control input which is the switching condition. For single input system, $u(\boldsymbol{x})$ is represented by $u^+(\boldsymbol{x})$ if $s(\boldsymbol{x}) > 0$ and $u^-(\boldsymbol{x})$ if $s(\boldsymbol{x}) < 0$, where $s(\boldsymbol{x})$ is a switching function and $u^+(\boldsymbol{x}) \neq u^-(\boldsymbol{x})$. The design objective is to generate sliding mode in hyperspace $s(\boldsymbol{x}) = 0$, which is called a sliding surface.

The system trajectory around sliding surface $s(\boldsymbol{x}) \to 0$ is observed. When $s(\boldsymbol{x}) > 0$, $s(\boldsymbol{x})$ must decrease with time, i.e. $\dot{s}(\boldsymbol{x}) < 0$. When $s(\boldsymbol{x}) < 0$, $s(\boldsymbol{x})$ must increase with time, i.e. $\dot{s}(\boldsymbol{x}) > 0$. Therefore, the sliding condition $\lim_{s \to 0} s\dot{s} < 0$ is satisfied. In order to arrive at sliding mode in finite time, this study defines the approaching condition [13]

$$\boldsymbol{s}^T \dot{\boldsymbol{s}} < -\sigma \left\| \boldsymbol{s} \right\| \quad \text{as} \quad \boldsymbol{s} \neq \boldsymbol{0}, \ \ \sigma > 0 \tag{1}$$

3.2 Design of Sliding-Mode Controller

According to the approaching and sliding conditions, two steps are carried out in designing a sliding-mode controller. First, choose a sliding function $\boldsymbol{s}(\boldsymbol{x})$ to make the system trajectory slide toward control objective in sliding mode. Second, determine control rule $\boldsymbol{u}$, which enforces the system trajectory to approach a sliding surface in finite time and in sliding mode. The design sequences of these two steps are opposite to behavior sequences of the system. In step 1, this study assumes the system has been controlled successfully on the sliding mode, and chooses an appropriate sliding function to ensure stability of the system. In step 2, control rules are determined to ensure the existence of an approaching mode and to produce the sliding mode.

Based on the pole-assignment design method [14], this study uses state space with gain feedback and moves closed-loop poles to desired positions. Consider a linear time invariant system:

$$\dot{\boldsymbol{x}} = \boldsymbol{A}\boldsymbol{x} + \boldsymbol{B}\boldsymbol{u} + \boldsymbol{d}(\boldsymbol{x}, t) \tag{2}$$

$$\boldsymbol{y} = \boldsymbol{H}\boldsymbol{x}$$

where $\boldsymbol{d}(\boldsymbol{x}, t)$ denotes disturbance and $\boldsymbol{u} \in \Re^m$ is a control input $(n > m)$. In addition, the system is controllable and $\boldsymbol{B} \in \Re^{n \times m}$ is assumed to be of full rank, i.e., $rank(\boldsymbol{B}) = m$.

Conventional sliding-mode controller design often requires choosing the sliding vector, a sliding surface $\boldsymbol{s} \in \Re^m$ is written as

$$\boldsymbol{s} = \boldsymbol{C}\boldsymbol{x} \tag{3}$$

where $\boldsymbol{C} \in \Re^{m \times n}$ is a sliding vector.

According to the pole-assignment method, the control input is designed as

$$\boldsymbol{u} = -\boldsymbol{K}\boldsymbol{x} \tag{4}$$

where $\boldsymbol{K} \in \Re^n$ is a gain matrix. Substituting Eq. (4) into Eq. (2) yields

$$\dot{\boldsymbol{x}} = \boldsymbol{A}\boldsymbol{x} + \boldsymbol{B}(-\boldsymbol{K}\boldsymbol{x}) + \boldsymbol{d}(\boldsymbol{x}, t) = (\boldsymbol{A} - \boldsymbol{B}\boldsymbol{K})\boldsymbol{x} + \boldsymbol{d}(\boldsymbol{x}, t) \tag{5}$$

The gain matrix $\boldsymbol{K}$ can be obtained by assigning n desired eigenvalues for the matrix $\boldsymbol{A} - \boldsymbol{B}\boldsymbol{K}$. For convenience, these eigenvalues are partitioned into $\{\lambda_1 \ \lambda_2 \ \cdots \ \lambda_{n-m}\}$ and $\{\omega_1 \ \omega_2 \ \cdots \ \omega_m\}$. To design sliding-mode controllers, a sliding function is designed first. The proposed sliding-mode controller is based on pole-assignment. As pole-assignment is employed to design a controller, in order to design an appropriate sliding vector $\boldsymbol{C}$, eigenvalues must satisfy conditions:

A. $\mathrm{Re}(\lambda_i) < 0$, $\omega_j \in R$, $\omega_j < 0$, $\lambda_i \neq \omega_j$.

B. The number of any repeated eigenvalue n is not greater than m.

C. $\{\omega_1 \ \omega_2 \ \cdots \ \omega_m\}$ are not in eigenvalues of matrix $\boldsymbol{A}$.

Sinswat and Fallside [15] presented that if Condition B exists, the controlled matrix $\boldsymbol{A} - \boldsymbol{B}\boldsymbol{K}$ can be diagonalized as

$$\boldsymbol{A} - \boldsymbol{B}\boldsymbol{K} = \begin{bmatrix} \boldsymbol{V} \\ \boldsymbol{C} \end{bmatrix}^{-1} \begin{bmatrix} \boldsymbol{J} & \boldsymbol{0} \\ \boldsymbol{0} & \boldsymbol{\Omega} \end{bmatrix} \begin{bmatrix} \boldsymbol{V} \\ \boldsymbol{C} \end{bmatrix} \tag{6}$$

where $\boldsymbol{J} = diag\{\lambda_1 \ \ \lambda_2 \ \cdots \ \lambda_{n-m}\}$, $\boldsymbol{\Omega} = diag\{\omega_1 \ \ \omega_2 \ \cdots \ \omega_m\}$, and $\boldsymbol{V} = [v_1 \ \ v_2 \ \cdots \ v_{n-m}]^T$, $\boldsymbol{C} = [c_1 \ \ c_2 \ \cdots \ c_m]^T$ are the left eigenvector with respect to $\boldsymbol{J}$ and $\boldsymbol{\Omega}$. Eq. (6) can be written as

$$\begin{bmatrix} \boldsymbol{V} \\ \boldsymbol{C} \end{bmatrix} (\boldsymbol{A} - \boldsymbol{BK}) = \begin{bmatrix} \boldsymbol{J} & \boldsymbol{0} \\ \boldsymbol{0} & \boldsymbol{\Omega} \end{bmatrix} \begin{bmatrix} \boldsymbol{V} \\ \boldsymbol{C} \end{bmatrix} \tag{7}$$

or

$$\boldsymbol{V}(\boldsymbol{A} - \boldsymbol{BK}) = \boldsymbol{JV} \tag{8}$$

$$\boldsymbol{C}(\boldsymbol{A} - \boldsymbol{BK}) = \boldsymbol{\Omega C} \tag{9}$$

Thus,

$$\boldsymbol{CA} - \boldsymbol{\Omega C} = \boldsymbol{CBK} \tag{10}$$

Since $\boldsymbol{C}$ contains m independent left eigenvectors, this study is $Rank(\boldsymbol{C}) = m$. Under conforming to Condition C of eigenvalues ω_i, $Rank(\boldsymbol{CA} - \boldsymbol{\Omega C}) = m$. It follows from Eq. (10) that $Rank(\boldsymbol{CBK}) = m$ and $Rank(\boldsymbol{CB}) \geq m$. Since $\boldsymbol{CB}$ is a $m \times m$ matrix, $Rank(\boldsymbol{CB}) \leq m$. Thus, $Rank(\boldsymbol{CB}) = m$ is obtained. In other words, $\boldsymbol{CB}$ is invertible and $\det(\boldsymbol{CB}) \neq 0$.

Define SMC as

$$\boldsymbol{u} = -\boldsymbol{Kx} + \boldsymbol{u}_s \tag{11}$$

where $\boldsymbol{u}_s$ is SMC input. Substituting Eq. (11) into Eq. (2) yields

$$\dot{\boldsymbol{x}} = (\boldsymbol{A} - \boldsymbol{BK})\boldsymbol{x} + \boldsymbol{Bu}_s + \boldsymbol{d}(\boldsymbol{x}, t) \tag{12}$$

According to [14]

$$\boldsymbol{u}_s = -(\boldsymbol{CB})^{-1}\boldsymbol{Cd}(\boldsymbol{x}, t) \tag{13}$$

Substituting Eq. (13) into (12), multiplying $\boldsymbol{C}$, and using (9) with $\boldsymbol{s} = \boldsymbol{Cx} = 0$ lead to

$$\boldsymbol{C}\dot{\boldsymbol{x}} = \boldsymbol{\Omega Cx} = 0 \tag{14}$$

or

$$c_i\dot{\boldsymbol{x}} = \omega_i c_i \boldsymbol{x} = 0 \tag{15}$$

Although eigenvalues ω_i can not affect sliding mode, in order to adjust the approaching speed in sliding mode, this study add the condition $\omega_j < 0$ to enforce the system to conform to sliding condition. Differentiating Eq. (3), using Eq. (12) and employing Eq. (9) lead to

$$\dot{\boldsymbol{s}} = \boldsymbol{C}\dot{\boldsymbol{x}} = \boldsymbol{C}(\boldsymbol{A} - \boldsymbol{BK})\boldsymbol{x} + \boldsymbol{CBu}_s + \boldsymbol{Cd}(\boldsymbol{x},t) = \boldsymbol{\Omega s} + \boldsymbol{CBu}_s + \boldsymbol{Cd}(\boldsymbol{x},t) \tag{16}$$

Define [16]

$$\begin{aligned} \boldsymbol{u}_s &= -(\|\boldsymbol{C}\|\delta(\boldsymbol{x},t) + \sigma)(\boldsymbol{CB})^{-1}\boldsymbol{sat}(\boldsymbol{s},\varepsilon) \\ &= -(\gamma + \sigma)(\boldsymbol{CB})^{-1}\boldsymbol{sat}(\boldsymbol{s},\varepsilon) \\ &= -\boldsymbol{Q}\cdot\boldsymbol{sat}(\boldsymbol{s},\varepsilon) \end{aligned} \tag{17}$$

where

$$\boldsymbol{sat}(\boldsymbol{s},\varepsilon) = \begin{cases} \boldsymbol{s}/\|\boldsymbol{s}\|, \text{ when } \|\boldsymbol{s}\| > \varepsilon \\ \boldsymbol{s}/\varepsilon, \text{ when } \|\boldsymbol{s}\| \le \varepsilon \end{cases} \tag{18}$$

and $\delta(\boldsymbol{x},t) \ge \|d(\boldsymbol{x},t)\|$ denotes the upper limit function of known disturbance. Moreover, σ is a positive constant, $\gamma = \|\boldsymbol{C}\|\delta(\boldsymbol{x},t)$, $(\gamma+\sigma)(\boldsymbol{CB})^{-1} = \boldsymbol{Q}$, and ε is small positive constant. Multiplying Eq. (16) by $\boldsymbol{s}^T$ to both sides and using Eq. (17) gives

$$\begin{aligned} \boldsymbol{s}^T\dot{\boldsymbol{s}} &= \boldsymbol{s}^T\boldsymbol{\Omega s} + \boldsymbol{s}^T\boldsymbol{CB}[-(\gamma+\sigma)(\boldsymbol{CB})^{-1}\boldsymbol{sat}(\boldsymbol{s},\varepsilon)] + \boldsymbol{s}^T\boldsymbol{Cd}(\boldsymbol{x},t) \\ &= \boldsymbol{s}^T\boldsymbol{\Omega s} - \boldsymbol{s}^T(\gamma+\sigma)\cdot\boldsymbol{sat}(\boldsymbol{s},\varepsilon) + \boldsymbol{s}^T\boldsymbol{Cd}(\boldsymbol{x},t) \\ &= \boldsymbol{s}^T\boldsymbol{\Omega s} - (\gamma+\sigma)[\boldsymbol{s}^T\cdot\boldsymbol{sat}(\boldsymbol{s},\varepsilon) - \boldsymbol{s}^T\boldsymbol{Cd}(\boldsymbol{x},t)/(\gamma+\sigma)] \end{aligned} \tag{19}$$

Since $\omega_j < 0$ according to Condition A, $\boldsymbol{s}^T\boldsymbol{\Omega s}$ is negative definite. The condition $\|\boldsymbol{Cd}(\boldsymbol{x},t)/(\gamma+\sigma)\| < 1$ is derived from $\gamma + \sigma > \|\boldsymbol{Cd}(\boldsymbol{x},t)\|$. In addition, $\gamma + \sigma > \|\boldsymbol{Cd}(\boldsymbol{x},t)\|$ is obtained by conditions $\gamma = \|\boldsymbol{C}\|\delta(\boldsymbol{x},t) \ge \|\boldsymbol{C}\|\cdot\|\boldsymbol{d}(\boldsymbol{x},t)\| \ge \|\boldsymbol{Cd}(\boldsymbol{x},t)\|$ and a positive constant σ. The condition $\boldsymbol{s}^T\cdot\boldsymbol{sat}(\boldsymbol{s},\varepsilon) - \boldsymbol{s}^T\boldsymbol{Cd}(\boldsymbol{x},t)/(\gamma+\sigma) > 0$ is confirmed by the condition $\gamma + \sigma \gg \varepsilon$. Thus, Eq. (19) satisfies $\boldsymbol{s}^T\dot{\boldsymbol{s}} < 0$. This condition represents that Eq. (1) is established. Hence, a sliding-mode controller

$$\boldsymbol{u} = -\boldsymbol{Kx} + \boldsymbol{u}_s = -\boldsymbol{Kx} - \boldsymbol{Q}\cdot\boldsymbol{sat}(\boldsymbol{s},\varepsilon) \tag{20}$$

is constructed to produce a stable sliding-mode system. Fig. 6(a) shows a block diagram using SMC.

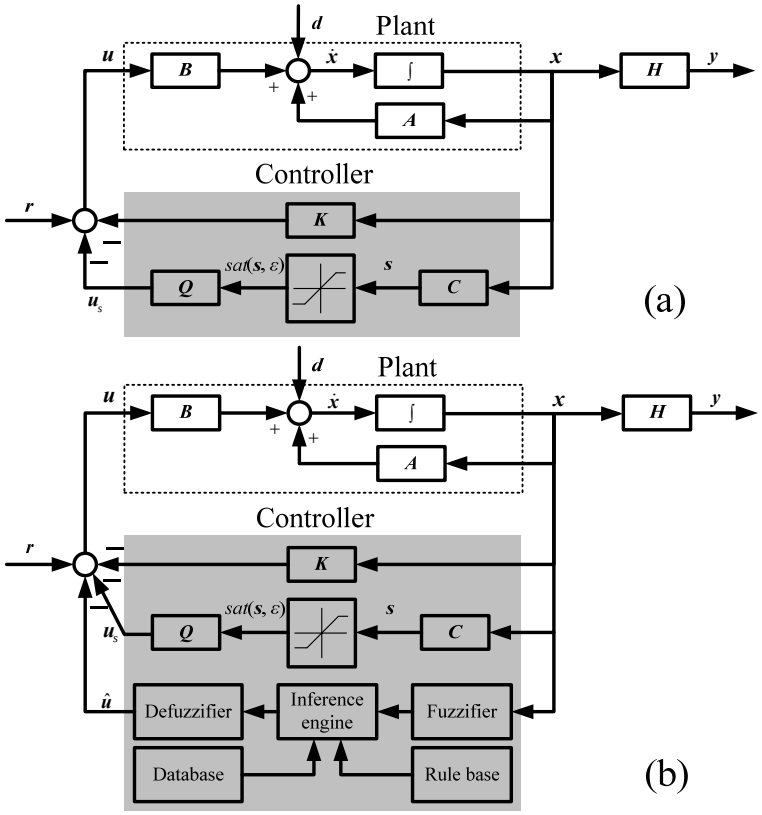

Fig. 6. Block diagram (a) with sliding-mode controller; (b) sliding mode based fuzzy controller.

3.3 Definitions and Assumptions of Fuzzy Control Input

Fig. 6(b) shows a block diagram using the sliding mode based fuzzy control. Triangular membership functions are used for three linguistic variables of inputs and the output, as shown in Fig. 7. Correlations between the input variables and the output variable are constructed into a rule base as shown in Table 2 for the output $\hat{\boldsymbol{u}}$. This study uses Mamdani's minimum fuzzy implication rule for the fuzzy inference and a center of area strategy in defuzzification for the possibility distribution of the output $\hat{\boldsymbol{u}}$.

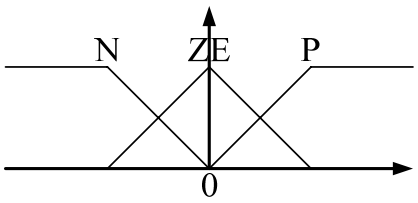

Fig. 7. Membership function.

Table 2: Fuzzy rules for output $\hat{\boldsymbol{u}}$ with inputs x_1 as displacement and x_2 as velocity.

	x_2		
x_1	N	ZE	P
P	ZE	P	P
ZE	N	ZE	P
N	N	N	ZE

3.4 SLIDING MODE BASED FUZZY CONTROL

Sliding mode based fuzzy control (SMBFC) is constructed by added a fuzzy control input $\hat{\boldsymbol{u}}$ based on the sliding vector $\boldsymbol{C}$ in Eq. (3) into the SMC. Adding fuzzy control input $\hat{\boldsymbol{u}}$ into Eq. (20) gives

$$\boldsymbol{u} = -\boldsymbol{K}\boldsymbol{x} - \boldsymbol{Q}\cdot\boldsymbol{sat}(\boldsymbol{s},\varepsilon) + \hat{\boldsymbol{u}} \quad = -\boldsymbol{K}\boldsymbol{x} - \boldsymbol{Q}'\cdot\boldsymbol{sat}(\boldsymbol{s},\varepsilon) \tag{21}$$

To fine tune $\boldsymbol{Q}\cdot\boldsymbol{sat}(\boldsymbol{s},\varepsilon)$ derived from SMC, this study combines $\hat{\boldsymbol{u}}$ with $\boldsymbol{Q}\cdot\boldsymbol{sat}(\boldsymbol{s},\varepsilon)$ to generate a new $\boldsymbol{Q}'\cdot\boldsymbol{sat}(\boldsymbol{s},\varepsilon)$. Assuming $\dot{\boldsymbol{x}} = \boldsymbol{A}\boldsymbol{x} + \boldsymbol{B}\boldsymbol{u} + \boldsymbol{d}(\boldsymbol{x},t)$ and using Eq. (21) with Eq. (17) lead to

$$\begin{aligned}\dot{\boldsymbol{x}} &= \boldsymbol{A}\boldsymbol{x} + \boldsymbol{B}\boldsymbol{u} + \boldsymbol{d}(\boldsymbol{x},t)\\ &= \boldsymbol{A}\boldsymbol{x} + \boldsymbol{B}[-\boldsymbol{K}\boldsymbol{x} - (\gamma+\sigma)(\boldsymbol{C}\boldsymbol{B})^{-1}\boldsymbol{sat}(\boldsymbol{s},\varepsilon) + \hat{\boldsymbol{u}}] + \boldsymbol{d}(\boldsymbol{x},t)\\ &= (\boldsymbol{A}-\boldsymbol{B}\boldsymbol{K})\boldsymbol{x} - \boldsymbol{B}[(\gamma+\sigma)(\boldsymbol{C}\boldsymbol{B})^{-1}\boldsymbol{sat}(\boldsymbol{s},\varepsilon) - \hat{\boldsymbol{u}}] + \boldsymbol{d}(\boldsymbol{x},t)\end{aligned} \tag{22}$$

For the ease of derivation, let $\hat{\boldsymbol{u}} = -(\boldsymbol{C}\boldsymbol{B})^{-1}\boldsymbol{C}\boldsymbol{x}$ as fuzzy control input, Eq. (22) becomes

$$\begin{aligned}\dot{\boldsymbol{x}} &= \boldsymbol{A}\boldsymbol{x} + \boldsymbol{B}[-\boldsymbol{K}\boldsymbol{x} - (\gamma+\sigma)(\boldsymbol{C}\boldsymbol{B})^{-1}\boldsymbol{sat}(\boldsymbol{s},\varepsilon) - (\boldsymbol{C}\boldsymbol{B})^{-1}\boldsymbol{C}\boldsymbol{x}] + \boldsymbol{d}(\boldsymbol{x},t)\\ &= (\boldsymbol{A}-\boldsymbol{B}\boldsymbol{K})\boldsymbol{x} - \boldsymbol{B}[(\gamma+\sigma)\cdot\boldsymbol{sat}(\boldsymbol{s},\varepsilon) + \boldsymbol{C}\boldsymbol{x}](\boldsymbol{C}\boldsymbol{B})^{-1} + \boldsymbol{d}(\boldsymbol{x},t)\end{aligned} \tag{23}$$

Differentiating Eq. (3) and using Eq. (23) lead to

$$\begin{aligned}\dot{\boldsymbol{s}} &= \boldsymbol{C}\dot{\boldsymbol{x}} \\ &= \boldsymbol{C}\{(\boldsymbol{A}-\boldsymbol{B}\boldsymbol{K})\boldsymbol{x}-\boldsymbol{B}[(\gamma+\sigma)\cdot\boldsymbol{sat}(\boldsymbol{s},\varepsilon)+\boldsymbol{C}\boldsymbol{x}](\boldsymbol{C}\boldsymbol{B})^{-1}+\boldsymbol{d}(\boldsymbol{x},t)\} \\ &= \boldsymbol{C}(\boldsymbol{A}-\boldsymbol{B}\boldsymbol{K})\boldsymbol{x}-[(\gamma+\sigma)\cdot\boldsymbol{sat}(\boldsymbol{s},\varepsilon)+\boldsymbol{C}\boldsymbol{x}]+\boldsymbol{C}\boldsymbol{d}(\boldsymbol{x},t) \\ &= \boldsymbol{\Omega}\boldsymbol{C}\boldsymbol{x}-[(\gamma+\sigma)\cdot\boldsymbol{sat}(\boldsymbol{s},\varepsilon)-\boldsymbol{C}\boldsymbol{d}(\boldsymbol{x},t)]-\boldsymbol{C}\boldsymbol{x} \\ &= \boldsymbol{\Omega}\boldsymbol{s}-[(\gamma+\sigma)\cdot\boldsymbol{sat}(\boldsymbol{s},\varepsilon)-\boldsymbol{C}\boldsymbol{d}(\boldsymbol{x},t)]-\boldsymbol{s}\end{aligned} \quad . \qquad (24)$$

Multiplying $\boldsymbol{s}^T$ to both sides of Eq. (24) gives

$$\begin{aligned}\boldsymbol{s}^T\dot{\boldsymbol{s}} &= \boldsymbol{s}^T\{\boldsymbol{\Omega}\boldsymbol{s}-[(\gamma+\sigma)\cdot\boldsymbol{sat}(\boldsymbol{s},\varepsilon)-\boldsymbol{C}\boldsymbol{d}(\boldsymbol{x},t)]-\boldsymbol{s}\} \\ &= \boldsymbol{s}^T\boldsymbol{\Omega}\boldsymbol{s}-\boldsymbol{s}^T[(\gamma+\sigma)\boldsymbol{sat}(\boldsymbol{s},\varepsilon)-\boldsymbol{C}\boldsymbol{d}(\boldsymbol{x},t)]-\boldsymbol{s}^T\boldsymbol{s} \\ &= \boldsymbol{s}^T\boldsymbol{\Omega}\boldsymbol{s}-(\gamma+\sigma)[\boldsymbol{s}^T\cdot\boldsymbol{sat}(\boldsymbol{s},\varepsilon)-\boldsymbol{s}^T\boldsymbol{C}\boldsymbol{d}(\boldsymbol{x},t)/(\gamma+\sigma)]-\boldsymbol{s}^T\boldsymbol{s}\end{aligned} \qquad (25)$$

Since $\boldsymbol{s}^T\boldsymbol{s}>0$ and $\boldsymbol{s}^T\boldsymbol{\Omega}\boldsymbol{s}-(\gamma+\sigma)[\boldsymbol{s}^T\cdot\boldsymbol{sat}(\boldsymbol{s},\varepsilon)-\boldsymbol{s}^T\boldsymbol{C}\boldsymbol{d}(\boldsymbol{x},t)/(\gamma+\sigma)]<0$ confirmed by Eq. 19, Eq. (25) can arrive at the approaching condition. Moreover, $-\boldsymbol{s}^T\boldsymbol{s}$ is an extra term in Eq. (25) in contrast to Eq. (19), which results in a faster approaching condition in SMBFC than in SMC. Therefore, SMBFC satisfies the approaching condition of SMC. Hence, SMBFC is constructed in Eq. (21). In Section 4, both SMC and SMBFC performances are compared.

4. SIMULATION RESULTS

Simulation results are shown in Fig. 8, where solid and dashed curves are results of SMC and SMBFC, respectively. The initial displacement is 2 μm and initial velocity is zero. Simulation results show that the settling time is 0.02 s by using SMBFC, whereas over 0.2 s using SMC. Moreover, the control input of SMBFC is less than that of SMC.

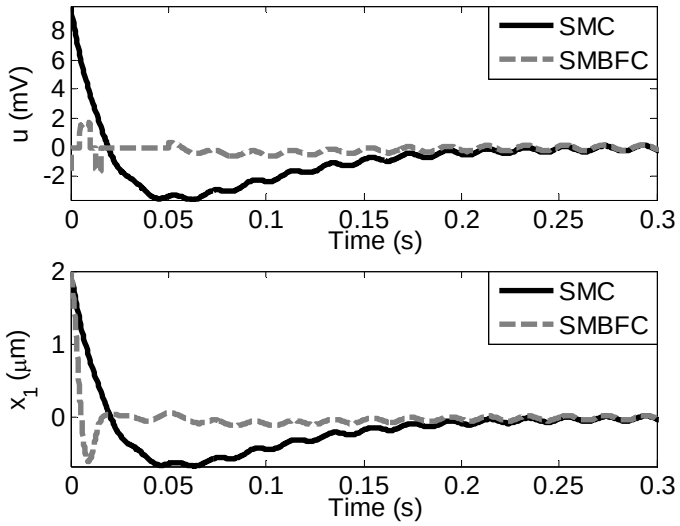

Fig. 8. Comparison of simulation results in control input u and displacement x_1.

5. EXPERIMENTAL SETUP AND RESULTS

The experimental setup consists of a modified pickup head, LDV, an analog-to-digital or digital-to-analog converter (AD/DA) card, and a personal computer to perform real-time control at a sampling rate of 10 kHz. Fig. 9 depicts a flowchart where y_D is the actuator displacement along the laser focusing direction.

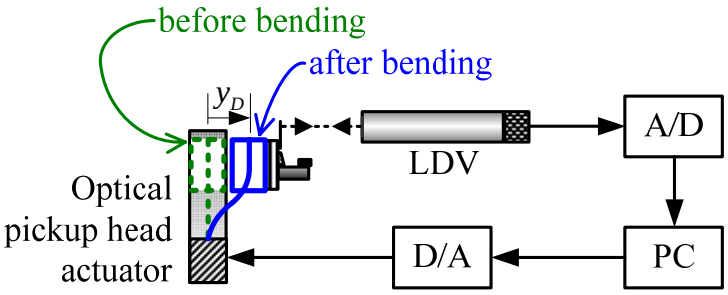

Fig. 9. Experimental setup: steel wire bent by Lorentz force and actuator focusing displacement y_D measured by LDV.

Experimental results using both controllers are compared in Fig. 10, where solid and dashed curves are results of SMC and SMBFC, respectively. The step response of 2 μm displacement and its error intensity spectrum between 0.5 s to 1 s are shown in Figs. 10 (a)

and 10 (b), respectively. The controller is not turned on until 0.5 s. The settling time of the system is 0.05 s by using SMBFC, whereas SMC needs 0.1 s. Moreover, the resonance in the error intensity spectrum of SMBFC is less than that of SMC.

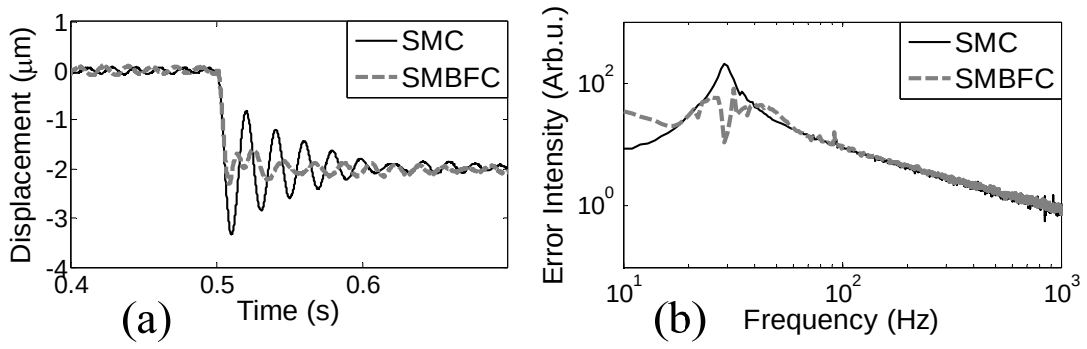

Fig. 10. Comparison of experimental results: (a) step response of 2 μm displacement at 0.5 s in control command and (b) error intensity spectrum obtained from 0.5 s to 1 s.

6. CONCLUSION

This study demonstrates the sensing displacement capability of the LD package as a displacement sensor by using the SMI signal. This study has presented the design of SMBFC, which has been proved to satisfy the approaching condition of SMC. Simulation results show that SMBFC requires less control input and yields faster response. Experimental results show that the step response of SMBFC is faster than that of SMC. The spectrum also shows that SMBFC yields smaller error than that of SMC.

7. ACKNOWLEDGEMENTS

This research was supported by National Science Council, Taiwan, under Grant No. NSC93-2752-E009-009-PAE.

REFERENCES

[1] Lee, D. J., Park, S. J., Woo, K. S., Park, N. C., and Park, Y. P. (2005). Design and analysis of two-wire focusing actuator for small-sized ODD with linear VCM type's actuator. Microsyst. Technol., 11, 470-477.

[2] Edwards, C and Tan, C. P. (2006). Sensor fault tolerant control using sliding mode observers. Control Engineering Practice, 14, 897-908.

[3] Allen, M., Bernilli-Zazzera, F., and Scattolini, R. (2000). Sliding control of a large flexible space structure. Control Engineering Practice, 8, 861-871.

[4] Zadeh, L. A. (1965). Fuzzy sets. Information and Control, 8(3), 338-353.

[5] Zulfatman and Rahmat, M. F. (2009). Application of self-tuning fuzzy PID controller on industrial hydraulic actuator using system identification approach. International Journal on Smart Sensing and Intelligent Systems, 2(2), 246-261.

[6] Wang, T. M., Liao, I. J., Liao, J. C., Suen, T. W., and Lee, W. T. (2009). An intelligent fuzzy controller for air-condition with Zigbee sensors. International Journal on Smart Sensing and Intelligent Systems, 2(4), 636-652.

[7] Hong, D., Hwang, I., Yoon, P., and Huh, K. (2008). Development of a vehicle stability control system using brake-by-wire actuators. J. Dynamic Systems, Measurement, and Control, 130, 011008-1-011008-9.

[8] Yagiz, N., Hacioglu, Y., and Taskin, Y. (2008). Fuzzy sliding-mode control of active suspensions. IEEE Trans. Industrial Electronics, 55(11), 3883-3890.

[9] Tsai, M. Y., Liu, T. S., and Schlesinger, T. E. (2009). Laser diode feedback signal for position sensing using self-mixing interference. Jpn. J. Appl. Phys., 48, 03A007-1-03A007-3.

[10] Giuliani, G., Norgia, M., Donati, S., and Bosch, T. (2002). Laser diode self-mixing technique for sensing applications. J. Opt. A: Pure Appl. Opt., 4, S283-S294.

[11] Neduncheliyan, S., Umapathy, M., and Ezhilarasi, D. (2009). Simultaneous periodic output feedback control for piezoelectric actuated structures using interval methods. International Journal on Smart Sensing and Intelligent Systems, 2(3), 417-431.

[12] Utkin, V. I. (1993). Sliding mode control design principles and applications to electric drives. IEEE Trans. Industrial Electronics, 40(1), 23-36.

[13] Baily, E. and Arapostathis, A. (1987). Simple sliding mode control scheme applied to robot manipulator. Int. J. Control, 45, 1197-1209.

[14] Chang, J. L. and Chen, Y. P. (2000). Sliding vector design based on the pole-assignment method. Asian J. Control, 2(1), 10-15.

[15] Sinswat, V. and Fallside, F. (1977). Eigenvalue/eigenvector assignment by state feedback. Int. J. Control, 23, 183-196.

[16] Slotine, J. J. E. and Sastry, S. S. (1983). Tracking control of nonlinear systems using sliding surfaces with application to robot manipulators. Int. J. Control, 38, 465-492.